DIGITAL EXCAVATION OF PALEOLITHIC OSSEOUS ARTIFACT

EMBEDDED IN BONE

An Undergraduate Research Scholars Thesis

by

ZACHARY A. NEWELL

Submitted to the Undergraduate Research Scholars program at
Texas A&M University
in partial fulfillment of the requirements for the designation as an

UNDERGRADUATE RESEARCH SCHOLAR

Approved by Research Advisor: Dr. Michael R. Waters

May 2020

Major: Anthropology

TABLE OF CONTENTS

ABSTRACT

Digital Excavation of Paleolithic Osseous Artifact Embedded in Bone

Zachary A. Newell
Department of Anthropology
Texas A&M University

Research Advisor: Dr. Michael R. Waters
Department of Anthropology
Texas A&M University

Micro computed tomography (micro-CT) and open source digital imaging and medical communication (DICOM) image processing software have great potential to study unique prehistoric artifacts. This is especially true for artifacts encased in concretions or embedded in other objects that cannot be physically excavated without destroying the artifact. Objects hidden from view can be made visible by obtaining micro-CT scans and then digitally excavating embedded objects in DICOM image processing software, such as 3D Slicer, through a process called segmentation. The 3D models produced by this process are then used to reconstruct the original form of the hidden objects using other 3D modeling software, in our case Blender. In cases where the physical removal of an embedded object threatens the destruction of the artifact, this non-invasive digital investigation may be the only way to study these unique artifacts. To demonstrate the utility of this methodology, a bone object, believed to be an osseous projectile point, found embedded in the rib of a 13,800 year old mastodon from the Manis site, Washington, is digitally excavated.

ACKNOWLEDGMENTS

Like most research, this project could not have been completed without the generous support of countless individuals and organizations. I have to start by giving a huge thank you to my faculty advisor and mentor Dr. Michael Waters for affording me the fantastic opportunities to work on such impactful projects at this early stage in my education and career. His exceptional guidance throughout this process has made me a better academic and will serve as a template for excellence that I can use to seek future mentors and become a mentor myself if I am ever so lucky to teach a future generation of archaeologists. I will never forget the lessons learned during my time working with him.

I would also like to thank the Center for the Study of the First Americans (CSFA) for funding this research. Micro-CT scans, 3D printing, and computers with enough processing power to efficiently process three-dimensional data do not come cheap, and, quite literally, this research could not have been conducted without the facilities and support provided by the CSFA. In addition, I appreciate the advice and input from Dr. Moreno, Dr. Robbins, and Ji-Wan Han over at the TAMU Biomechanical Environments Laboratory. Their software suggestions and assistance with getting me set up to do my research was invaluable and I am deeply thankful.

Finally, I would like to give a special thank you to my colleagues and mentors over at Prentice Thomas and Associates. These generous people gave me my first introduction to the world of archaeology, and I will forever be in their debt for awakening what will be my lifelong passion.

NOMENCLATURE

Micro-CT   Micro computed tomography

DICOM   Digital Imaging and Communications in Medicine

Voxel   A unit that represents a value on a regular three-dimensional grid space

Segmentation   A method of contouring used to delineate scanned objects of interest.

CHAPTER I

INTRODUCTION

The use of radiography to reveal the hidden contents of cultural materials can be traced back almost as far as the discovery of x-rays in 1895. Within just a few years of this discovery, the first fuzzy radiographs had already been taken of Egyptian mummies and their associated artifacts (Hughes 2011). Unfortunately, radiography did not become standard practice for many artifacts outside of mummies and paintings. Over a century of advancements in this technology vastly improved image quality of x-rays and stretched the possibilities for its uses. Development of digital computing paved the way for a more advanced method of x-ray imaging known as "Micro-Computed Tomography" (micro-CT). Micro-CT is a 3D imaging technique that captures hundreds of x-ray images, referred to as slices, of an object on multiple axes.

Publications demonstrating the implementation of micro-CT scans to analyze archaeological materials other than Egyptian mummies are relatively few and quite recent. Research presented in Nicholas et. al. (2014) exemplifies much of the work being done in Europe to produce 3D models of Iron Age artifacts with embedded components. They demonstrate how "Digital Imaging and Communications in Medicine" (DICOM) image processing software was used to create 3D volume renderings of a granite and iron counterweight as well as pottery vessels found in cremation burials. The physical models 3D printed from their renderings proved themselves invaluable in the analysis of the materials that would ordinarily need to have been extracted using destructive excavation in order to view them.

In a field that often deals with one-of-a-kind artifacts, archaeologists are regularly presented with the hard choice to either preserve an artifact for future research and verification or

to destroy an artifact in some way to gain information not accessible in any other way. Although some measurements currently have no alternative nondestructive techniques available, radiocarbon dating for example, there are plenty of ways that the modern archaeologist can and should be looking to implement nondestructive alternative measurement techniques wherever possible. Recent innovation in home computing has lowered the barrier to access processing power sufficient for the management and analysis of large packages of data such as those produced by micro-CT. This combined with a variety of open source DICOM image processing software available online, makes the 3D modeling of micro-CT data an excellent tool for revisiting debates halted by the need to preserve an artifact.

Micro-CT in Paleontology

Despite the limited examples of micro-CT scans being used to model obscured objects in the field of archaeology, these imaging and modeling techniques have found purchase within the paleontological community. Described as "Virtual Paleontology" by Rahman and Smith (2014), these cutting edge imaging techniques employ a broad spectrum of scanning technology, including but not limited to x-ray micro-CT, synchrotron-based tomography, and neutron tomography, to produce 3D models of "…poorly understood or previously unknown anatomies of fossil [life]…". Researchers within this field have been able to produce models of extinct creatures with enough precision that the data can be rigorously analyzed with the quantitative analysis of computer models.

By the very nature of paleontological research, most of their subject matter is deeply embedded in rock and the objects of interest are often quite fragile. When studying the particulars of an organism's anatomy, it is very important to preserve the positioning of articulated or semi-articulate fossils in order to best understand how specific skeletal systems

articulate with one another. Perhaps one of the most significant contributions these imaging techniques have made to the field of paleontology is their aid in the analysis of extinct organic remains that have been encapsulated in amber. The preservative qualities of amber make it an ideal material for studying the past and reconstructing ancient tropical environments because not only do small vertebrate organisms often become engulfed by the material, but so does a wide variety of insects, microorganisms such as pollen and fungal spores, and plant materials (Daza et. al. 2016). The high resolution imaging of virtual paleontology allows researchers to model and study even the smallest particles preserved through time.

Manis Mastodon

To demonstrate the utility of this methodology for archaeological purposes, I will apply them to the analysis of the Manis Mastodon site. Located on Washington's Olympic Peninsula, the Manis Mastodon site remains suspended in debate over its existence as either a landmark archaeological site, with potential to contribute to our understanding of early man in North America, or merely a paleontological site. A section of the semi-articulated skeletal remains of a 45-year-old mastodon, initially unearthed via backhoe by landowner Mr. Emanuel Manis, brought investigators to the site in 1977 (Gustafson et. al. 1979). Wet screening of the excavated backfill revealed the specimen of interest to this study: the head of a mastodon rib bone which appears to have the tip of an osseous projectile embedded in the dorsal surface of its proximal end (Figure 1). Further careful excavation revealed the left side of the mastodon to be in an articulated position in contact with the ground, while the right side was scattered a few meters away and exhibited signs of butchery (Gustafson et. al. 1979). Aside from a flaked cobble spall, no other artifacts were associated with the mastodon remains.
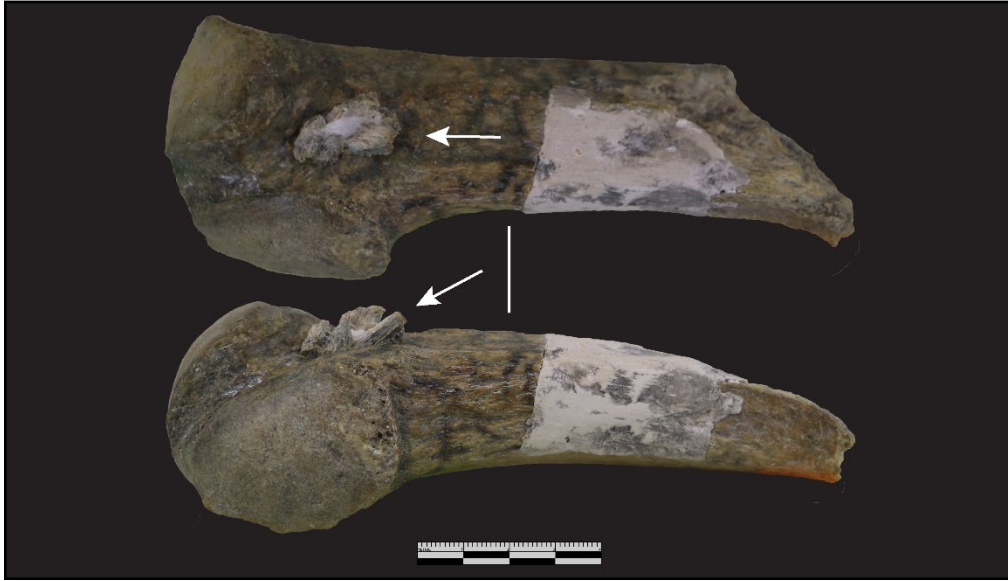
Figure 1. Manis Mastodon Rib. A fragment of the 14th rib of a 45-year-old mastodon with osseous inclusion near the head. Patches of white on the rib diaphysis and in the center of the embedded object are sites where samples were removed for radiocarbon dating and DNA sequencing. Arrows indicate trajectory of suspected projectile.

The rib of the Manis mastodon was reinvestigated in 2011 by Michael Waters and his team to evaluate the original date, of approximately 14,000 cal B.P., that was obtained from micro-organics in the soil by Gustafson and his team in the 1970's. Waters and his team also obtained high-resolution micro-CT scans of the embedded bone object, conducted DNA sequencing, and created rough models of the embedded object. Direct radiocarbon dates were obtained on the Manis rib and both mastodon tusks found at the site yielded a radiocarbon age of $11,960 \pm 17$ years B.P. (approximately 13,800 cal B.P.)(Waters et. al. 2011). The high-resolution micro-CT scans obtained for Waters' 2011 investigation, revealed the thin pointed profile of the osseous intrusion that measured approximately 3.5 cm in total length and penetrates 2.15 cm into the rib. These higher quality scans, obtained from the University of Texas High-Resolution X-ray Computed Tomography facility (UTCT) in 2011, provided a less ambiguous view of the intrusion than the simple x-rays taken in the late 1970's. The poor quality imaging available to

7

Gustafson and his team led them to conclude that there was evidence for bone healing at the site of injury, equivalent to about 4 to 5 months in human bone repair rates, suggesting an ante mortem introduction of this osseous intrusion — Waters and his team refute this claim based on evidence presented by their higher quality scans.

The DNA sequencing conducted by Waters (2011) was able to determine that the object embedded in the Manis mastodon rib was made of mastodon bone. This, combined with the more accurate age of 13,800 cal B.P., strongly suggests that there were people hunting proboscideans on the North American west coast approximately 800 years before the earliest accepted evidence of Clovis, a culture often proposed to be the first inhabitants of the continent.

Now that the Manis site has reliable dates and higher resolution two-dimensional imaging, the next stage in determining whether or not the embedded bone object is truly the result of pre-Clovis hunting activity is to precisely define the shape of the object and identify any features consistent with the intentional modification of bone by humans. The rough models produced by Waters and his team (2011) help with the general visualization of the embedded object, but this case proves to be an excellent candidate for the application of the more precise 3D modeling techniques employed in 'virtual paleontology' and the study of iron age artifacts. This study demonstrates the utility of advanced imaging and 3D modeling software for archaeological purposes by reanalyzing the bone object embedded in the Manis rib. The higher precision of this technique will be used to model the individual fragments of the embedded object, rather than the object as a whole, so that they can be refitted to accurately depict the true form of the embedded object.

CHAPTER II

METHODS

The first step in the analysis of embedded materials is obtaining images that accurately depict the obscured portions of the object. An effort to do so for the Manis mastodon rib was described in Gustafson et. al. (1979) when the first x-rays of the artifact were obtained. These low-resolution images were sufficient for determining that the bone inclusion was in fact the result of a puncture wound, but were not clear enough to give investigators any indication of the foreign object's morphology. Although high resolution micro-CT scans were obtained as a component of the investigation carried out by Waters and his team (2011), new micro-CT scans of the osseous intrusion were taken by the Texas A&M Mechanical Engineering Department specifically for the purposes of this reanalysis. These scans produced thousands of sequential thin sections of the artifact spaced 0.05901 mm apart at three perpendicular angles. These data, in their raw form, are represented by a stack of individual .TIFF files that are encoded with additional data that specifies the voxel dimensions and space between slices. Voxels are discrete units that represent a value on a regular three-dimensional grid and can be thought of as the three-dimensional equivalent of pixels. Although the images produced by the micro-CT scans we obtained as well as the ones Waters and his team (2011) provided, were much clearer than what was produced by Gustafson and his team in the 1970's, the ability to relay information about the overall shape of the embedded object is hindered by limitations of two-dimensional representation.

3D Slicer

To overcome the limitations of two-dimensional representations without going so far as to physically remove the embedded object, Waters and his team (2011) created a rough 3D digital model of the embedded object and the surrounding rib bone. Unfortunately, the rudimentary form made it difficult to differentiate between foreign bone fragments and local rib bone as well as identify individual fragments that make up the embedded object. In order to create a better model than what was presented in Waters (2011), open-source DICOM image processing software, 3D Slicer, was used to register the 2,067 individual slices of raw micro-CT data taken of the Manis bone intrusion. 3D Slicer's interactive viewport, shown in Figure 2, displays the axial, coronal, and sagittal slices of a scanned object that intersect with one another at any selected point within the object. This viewport was not only useful for visualizing the Manis rib in three dimensions, but was essential in the 3D modeling of the embedded object through a process called segmentation.
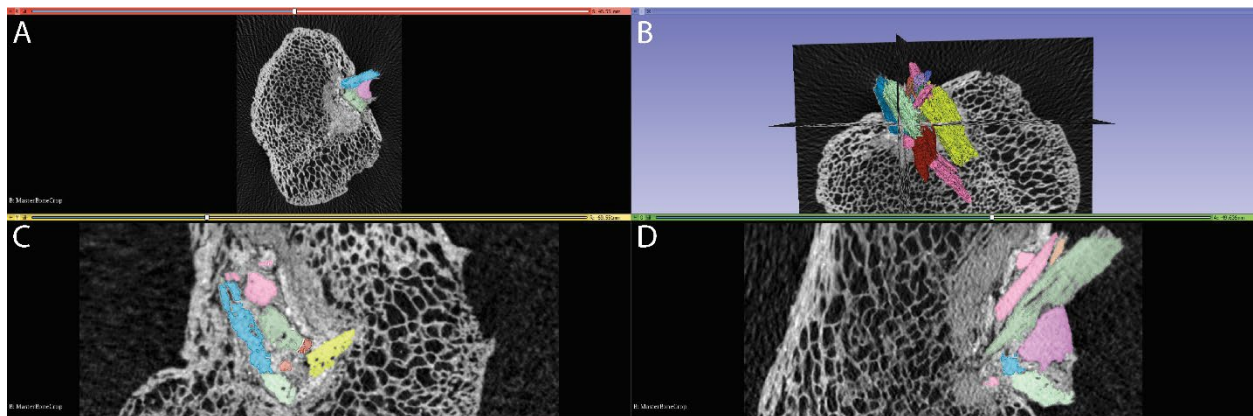
Figure 2. 3D Slicer Interactive Viewport. Three micro-CT cross sections of the Manis rib showing exterior cortical bone and the spongy interior trabecular bone. Colored areas represent the fragments of the intrusive object. (A) axial view, (B) volume rendering of embedded fragments (in color) and the intersecting axial, sagittal, and coronal plains depicted in A, C, and D, (C) sagittal view, (D) coronal view. Images are not to scale.

Segmentation is the process by which you can define, label, and find the volume of discrete portions of a scanned object. Variously colored labels, made up of voxels measuring 0.05901 mm^3, are painted two-dimensionally on each slice to mark the area of the profiles of discrete objects that are observed in the scan. As the profile of an object is continuously marked on sequential abutting slices, a volumetric model of the object is formed. In the medical field, this process is commonly employed to find the location, shape, and volume of tumors and foreign bodies within patients. In the case of the Manis mastodon rib, segmentation was used to determine the size, location, and orientation of each fragment that comprised the embedded osseous object.

In most cases, when micro-CT scans are taken of embedded foreign bodies, the differential makeup of the foreign object and whatever matrix it is suspended in produces varying grayscale values on the scan produced. This variation can then be exploited by 3D Slicer's algorithms to automatically segment an object based on its grayscale value that is unique from the surrounding tissue. However, since the embedded osseous inclusion is comprised of mammoth bone, as was determined by DNA sequencing (Waters et. al. 2011), it absorbs the same amount of x-rays as the rib tissue it is embedded in. Due to this phenomenon, the grayscale values of the rib tissue and the embedded osseous object were too similar to employ 3D Slicer's algorithms to automatically segment the foreign object fragments. As a result, each separate fragment had to be manually segmented by drawing the profile of every piece on all 2,067 individual slices.

This made the segmentation process for the object embedded in the Manis mastodon rib extremely time consuming. It took an estimated 500 hours for one individual to fully segment the suspected projectile and surrounding cortical bone of the rib manually. The time it takes to carry

out this process, of course depending on the size of the area of interest, would likely be reduced by as much as a factor of 10 if the density of the embedded material much greater than the host material.

While 3D Slicer has the ability to produce volumetric models of the embedded osseous object fragments, it does not have the ability to manipulate their positions. When labels are placed to define the shape of an object during segmentation, they are simply arrangements of voxels encoded with both the type of object they are designated to represent and their location in reference to fiducial markers. These data are not actual 3D objects that can be manipulated in space until a polygonal mesh is constructed of the model's surface when it's exported into another file type (e.g. .stl, .obj).

Blender

In order to refit the fragments that make up the osseous intrusion, the 3D models produced in 3D Slicer were processed in an open-source 3D modeling software called Blender. Used for a number of purposes ranging from digital sculpting to feature-length animations, Blender is a versatile platform that was well suited for making the fine adjustments necessary to reconstruct the original form of the osseous inclusion. Every fragment modeled in 3D Slicer was brought into Blender in the exact orientation and scale as they lie embedded in the mastodon rib, so as to best understand the relationships between each fragment before they are moved for refitting. The models of fragments segmented in 3D Slicer were refitted by making minor adjustments to each fragment's position and angle until they were attached to once central anchor piece that remained untouched. We chose segment 1, from Supplemental Table 1, to be this anchor piece because it was by far the largest piece.

In addition to the fragmented edges that match up with one another, an unexpected phenomenon was identified and used as a reference in the refitting process. A series of cylindrical voids, interpreted to be remnants of osteons, were observed within the vast majority of segmented fragments Figure 3. Osteons are cylindrical channels found within compact cortical bone that act as passages through which blood is moved throughout the bone. Since osteons run in the same direction throughout the bone, parallel to the long bone diaphysis, we paid careful attention to make sure that the osteons in each of the refitted fragments ran parallel with one another. We also made sure to only try and refit fragments if they were adjacent to each other in their in situ orientation. Once the reconstructed model of the osseous inclusion was complete, it was 3D printed using the Stratasys Eden260VS printer at 1:1, 2:1, and 3.5:1 scale for further analysis.
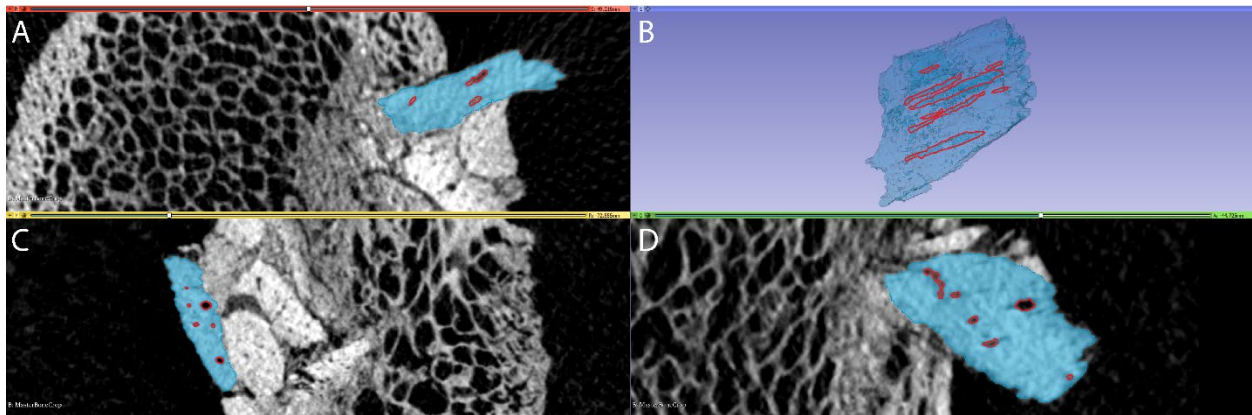
Figure 3. Osteons in Segment 7 Shown in Blue. This shows Segment 7 in 3D Slicer with osteons highlighted in red. (A) axial view, (B) volume rendering of Segment 7, (C) sagittal view, (D) coronal view. Images are not to scale.

CHAPTER III

RESULTS

Analysis of the Manis rib in 3D Slicer revealed a total of 24 foreign bone fragments embedded in the dorsal face of the proximal end of the rib. These fragments appear to be orientated in line with the rib diaphysis pointing toward the head of the rib at an approximate 30 degree downward angle. Of the 24 individual foreign fragments, 18 fragments, featured in color on Figure 4 and Supplemental Figure 9, were refitted with one another in an effort to reconstruct the foreign osseous object. The dimensions of these fragments, listed in Supplemental Table 1, range from 1.99 mm to 28.7 mm in length and penetrate a maximum depth of 2.15 cm into the porous trabecular bone of the rib. The six remaining fragments not included in the reconstruction of the osseous object were left out because they were too small and amorphous to confidently fit onto the reconstruction of the embedded osseous object. These omitted fragments only make up 1.05% of the total volume of foreign objects segmented, and likely had very little to contribute to the overall shape of the embedded object.
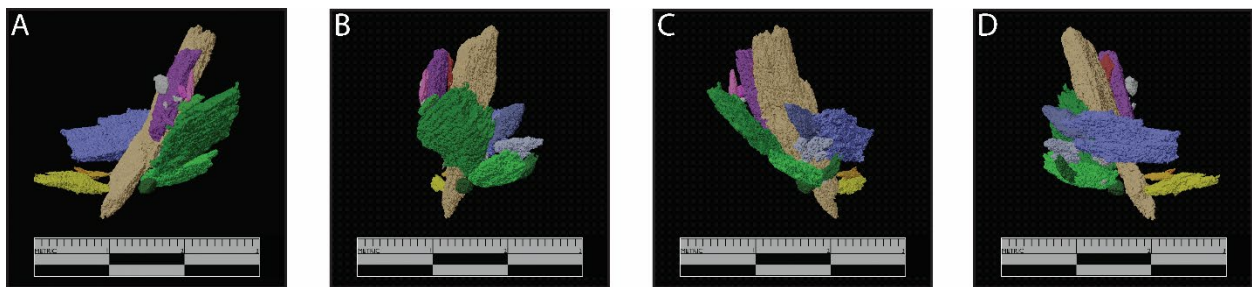
Figure 4. In Situ Projectile Fragments. A scale depiction of the pieces embedded in the Manis rib in their original orientation; colored pieces were used in the reconstruction while grey pieces were not used. See Supplemental Table 1 for the sizes of each fragment. A-D show the model as it is rotated clockwise.

In addition to the embedded osseous object, the surrounding cortical bone that comprises the wound entry was also segmented to ensure that all of the displaced local bone was accounted for and not included in our reconstruction of the suspected projectile. The wound opening, represented in Figure 5, has a max length and width of 20.2 mm and 9.86 mm, respectively. The cortical bone that was displaced by the suspected projectile impact, completely detached along the entire perimeter of the wound opening except for the edge closest to the shaft of the rib. This displaced cortical bone measures to the same dimensions as the wound opening and, like the suspected projectile, plunges into the rib's spongy trabecular bone at an approximate 30 degree downward angle pointed towards the rib's head. Beneath this displaced cortical bone, as well as in areas where the foreign object has penetrated the bone, an accumulation of gray material exists. As seen in Figure 6, this material is not as dense as the rib's cortical bone nor the embedded foreign object. This material is interpreted to be portions of the spongy trabecular bone matrix that was compacted as the suspected point displaced the rib's cortical bone downward. We prefer this interpretation over the one made in the 1970's using x-rays that claimed this material was evidence for bone healing.

The areas with the thickest accumulation of this material occur where the most trabecular bone would have been displaced, whereas regions adjacent to the impact zone that experienced little displacement of trabecular bone have little to no accumulation of this material. This is not consistent with a healing response to fractures typically seen in bone. After 4 to 5 months of healing, as suggested in (Gustafson et. al. 1979), a boney callus would form over the entire surface of the wound and bone remodeling would be well underway (Sheen and Garla 2019).
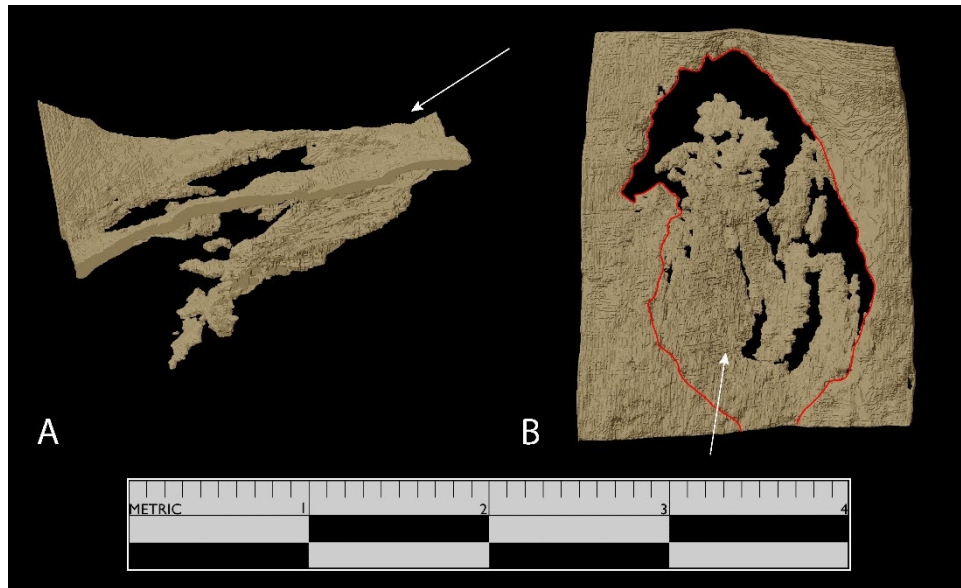
Figure 5. Manis Rib Wound. (A) side-view of the wound showing the displaced cortical bone position, (B) top-down view with wound perimeter outlined in red. The arrows indicate the trajectory of the projectile.
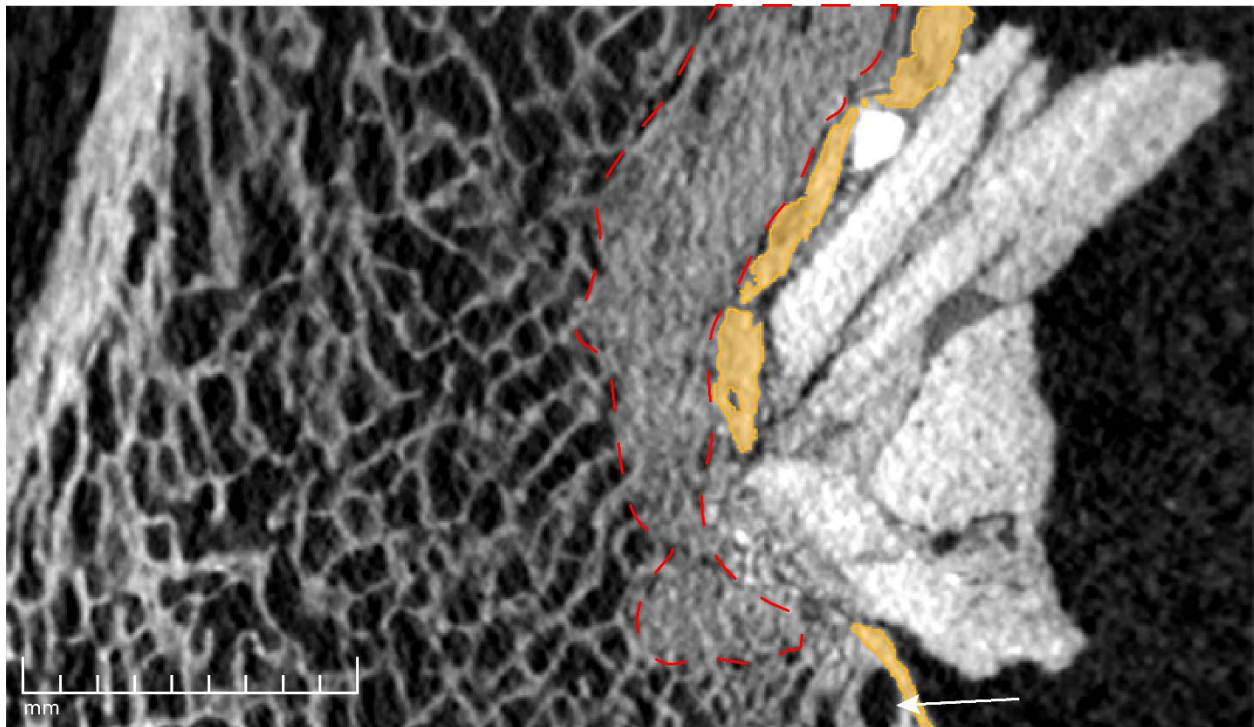
Figure 6. Trabecular Bone Compression. Pieces highlighted in orange represent displaced cortical bone from the rib. Crushed trabecular bone is outlined by a red dashed line. Note the unaffected trabecular bone below the zone pointed out by the white arrow.
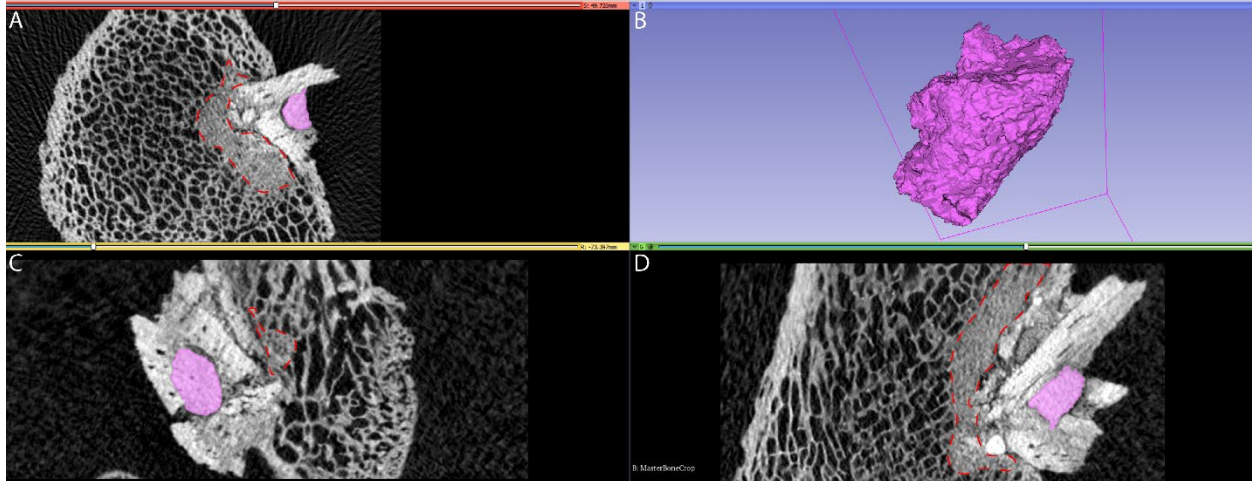
Figure 7. Bore Hole Cast Model. (A) axial slice, (B) 3D rendering of bore hole cast, (C) sagittal slice, (D) coronal slice. Crushed trabecular bone is outlined in red dashed line. Images are not to scale.

The accuracy of the segmentation process is shown in the model depicted in Figure 7. When the DNA sample was collected by Waters et. al. (2011), a 4mm diameter hole was drilled into the intrusive bone to collect bone powder for analysis. This hole was then filled with plaster, along with the segment of rib shaft that was removed to obtain a sample for radiocarbon dating. The model in Figure 7 shows the plaster cast of the bore hole drilled into the bone intrusion by Waters and his team (2011). From our segmentation of the cast—— left behind after filling the hole, we were able to confirm that investigators used a 4 mm bit to drill 6.8 mm into the center of the impact zone. The model shows that the artifact was drilled into twice, once at half depth and once at a different angle all the way to full depth. As seen in Figure 7, the sample taken also avoided drilling into any bone belonging to the rib itself, further supporting the claim that the sample removed, and tested positive for mastodon bone, is representative of the embedded object.

Reconstruction

Reconstruction of the osseous inclusion from the 18 pieces segmented in 3D Slicer produced a projectile point shaped model that measures 34.5 mm long, 16.9 mm wide, and 5.8 mm thick. This model, depicted in Figure 8 and Supplemental Figure 10, possesses three distinct features that lead us to believe that it is the tip fragment of an osseous projectile point. It has a: plano-convex cross-section, beveled lateral margin, and a preserved edge — all of which indicate intentional shaping. While the point was clearly broken at some point in the mid-section, evidenced by the fracture patterns on our model's proximal end, and there are missing fragments nearer to the distal end, there were enough refitting pieces to establish a cross-section of the point approximately 20 mm from the distal extremity. The cross-section depicted below side A in Figure 8 displays one relatively flat face, which we refer to as the ventral surface for the purposes of this discussion, and one clearly convex face, referred to as the dorsal face. The left lateral margin of the ventral face appears to be significantly beveled, thus deviating slightly from a perfectly flat surface. This beveled edge tapers to a sharp margin with an acute angle that is preserved by a single fragment, segment 14 in Supplemental Table 1.

Two burin-like fractures can be seen to extend 12.5 mm and 20 mm from the tip along the right and left side of our model, respectively, when looking at side A in Figure 8. These burinations, along with the highly fragmented state of the rest of the point, indicate that this inclusion most likely occurred as the result of a high-velocity impact event. We suspect that at the time of impact, the osseous projectile penetrated the mastodon soft tissue and collided with the rib bone with enough force that several pieces of the distal end immediately detached and became suspended in the soft tissue. The initial impact may have also caused a series of micro-fractures to occur throughout the rest of the point, which caused the projectile to fragment into

several pieces as it encountered resistance while penetrating the surface of the rib. Pieces that did

not remain attached long enough to enter the bone would not be preserved in the archaeological

record, and thus do not appear as a part of our model.
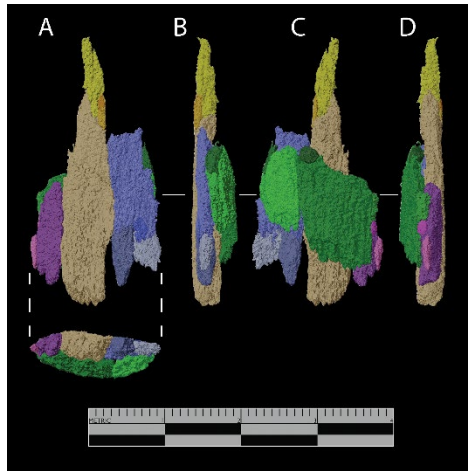
Figure 8. Manis Osseous Projectile Reconstruction. A scale depiction of the Manis osseous projectile reconstruction. (A) ventral face, (B) left lateral margin, (C) dorsal face, and (D) right lateral margin. See Supplemental Table 1 for the sizes of each fragment.

CHAPTER IV

CONCLUSION

This study shows the utility of implementing current medical imaging methods and DICOM image processing software to analyze unique archaeological specimens that feature obscured components. In cases where the obscured components cannot be removed without destroying the artifact for future studies or the relative position and context of the embedded objects are important, such as in the case of the Manis mastodon rib, this methodology could be the only way to extract important archaeological information from the artifact. It is for these reasons that archaeologists need to adopt these methods with the same level of enthusiasm as the paleontological community.

Although they may not have all of the same features as their expensive alternatives, we chose to use both 3D Slicer and Blender because they were open-source, and to prove that the operating cost for these techniques is relatively low. Admittedly, the cost to acquire high-resolution micro-CT scans is not low, however, this service is becoming more accessible, higher quality, and less expensive every year. The fact that 3D Slicer and Blender are free, can help offset the cost to acquire the highest quality scans possible. As mentioned earlier, this study required an extensive investment of labor to manually segment each of the embedded projectile fragments. However, this cost may be unique to the artifact in focus for this study, due to the very similar densities of material being segmented. If these techniques were applied to a bone that had either an ivory or stone projectile embedded in it, the bulk of the segmentation could be carried out automatically using Slicer's algorithms.

Despite the drawback of needing to do all of the work manually, the end result of using these techniques to analyze the Manis mastodon rib was quite satisfactory. This study was able to go beyond the previous 40 years of research at this site, and produce a highly accurate model of the embedded osseous projectile tip. The model has multiple recognizable characteristics of intentional modification and clearly resembles the morphology of a projectile. These techniques were even able demonstrate some unanticipated results that would never be apparent from simple visual examination. The discovery of osteons within the embedded fragments combined with the fact that the fragments are made out of mastodon bone, evidenced by DNA sequencing (Waters et. al. 2011), indicates that the osseous inclusion was constructed out of mastodon cortical bone, potentially narrowing down portions of the animal that could have been utilized to construct this projectile.

This exercise exemplifies the need in archaeology to constantly readdress our past interpretations of important archaeological finds using the latest technology available; as well as prioritizing non-destructive investigative techniques for the very reason that future technology can provide solutions to today's problems. I urge my colleagues to take stock of what techniques are being used in other fields that are tasked with solving similar problems, and find creative ways to apply them to this field. None of the software used in the production of our models was specifically designed to carry out the tasks we wanted to do, yet, these completely open-source programs were used to acquire a new perspective on an old problem that has paradigm shifting implications for how we look at the peopling of the Americas.

REFERENCES CITED

3D Slicer
      2020   Slicer 4.10.2. Electronic document, https://www.slicer.org/, accessed March 1,
          2020.

Daza, Juan D., Edward L. Stanley, Philipp Wagner, Aaron M. Bauer, and David A. Grimaldi
      2016   Mid-Cretaceous amber fossils illuminate the past diversity of tropical lizards.
          Science Advances 2(3):1-8.

Gustafson, Carl E., Delbert Gilbow, and Richard D. Daugherty
      1979   The Manis Mastodon Site: Early Man on the Olympic Peninsula. *Canadian*
          Journal of Archaeology 3:157-164.

Huges, Stephen
      2011   CT Scanning in Archaeology. *Computed Tomography – Special Applications,*
          Edited by Dr. Luca Saba, pp. 57-70.

Nicholas, Théophane, Ronan Gaugne, Cédric Taverneir, Valérie Gouranton, and Bruno Arnaldi
      2014   Preservative Approach to Study of Encased Archaeological Artefacts.
          International Conference on Cultural Heritage 332-341. Lemessos, Cyprus.

Rahman, Imran A. and Selena Y. Smith
      2014   Virtual Paleontology: Computer-Aided Analysis of Fossil Form and Function.
          Journal of Paleontology 88(4):633-635.

Sheen, Jonathan R. and Vishnu V. Garla
      2019   Fracture Healing Overview. National Center for Biotechnology Medicine,
          Electronic document, https://www.ncbi.nlm.nih.gov/pubmed/31869142, accessed
   March 20, 2020.

Waters, Michael R., Thomas W. Stafford Jr., H. Gregory McDonald, Carl Gustafson, Morten
Rasmusssen, Enrico Cappellini, Jesper V. Olsen, Damian Szklarczyk, Lars Juhl Jensen, M.
Thomas P. Gilbert, and Eske Willerslev
      2011   Pre-Clovis Mastodon Hunting 13,800 Years Ago at the Manis Site, Washington.
   *Science 34*:351-353.

SUPPLEMENTAL MATERIAL

Supplemental Table 1. Segment Size and Color.

Segment Number	Color	Length (mm)	Width (mm)	Thickness (mm)
1		28.70	6.73	3.39
2		2.06	0.857	0.293
3		4.74	0.995	1.00
4		10.50	2.22	1.86
5		2.43	1.94	1.90
6		4.56	1.81	1.40
7		14.10	11.30	2.14
8		3.90	1.60	0.723
9		11.10	5.69	2.09
10		6.39	2.29	0.532
11		2.50	0.713	0.415
12		12.6	3.57	1.75
13		1.99	0.965	0.801
14		4.32	1.14	0.699
15		8.30	3.07	2.16
16		17.20	5.67	2.46
17		3.23	1.55	0.627
18		6.43	3.72	1.29
19		3.43	1.79	1.59
20		2.89	1.34	0.788
21		1.38	0.655	0.445
22		0.985	0.746	0.348
23		2.20	0.649	0.343
24		0.927	0.727	0.429
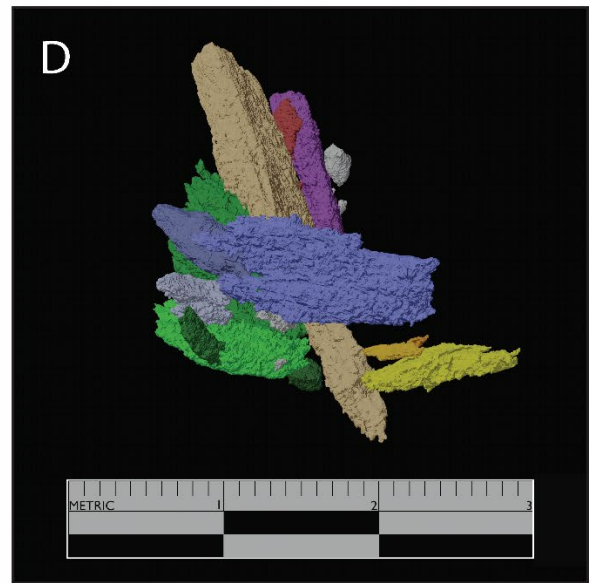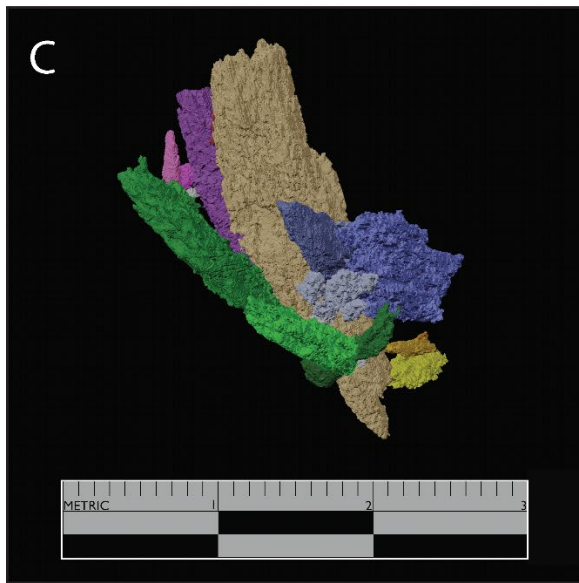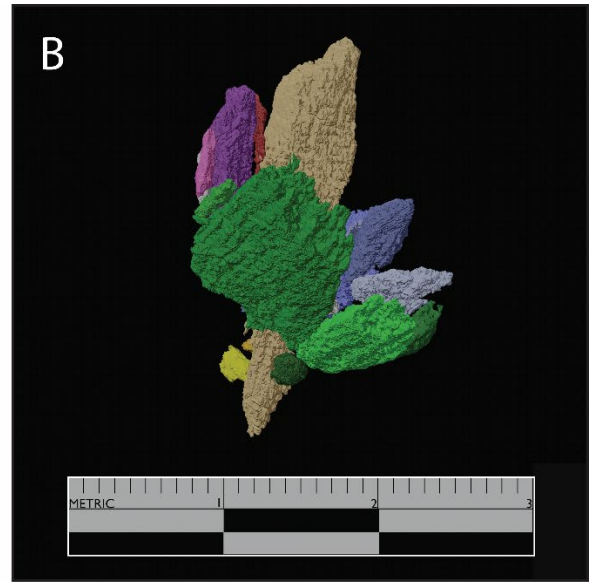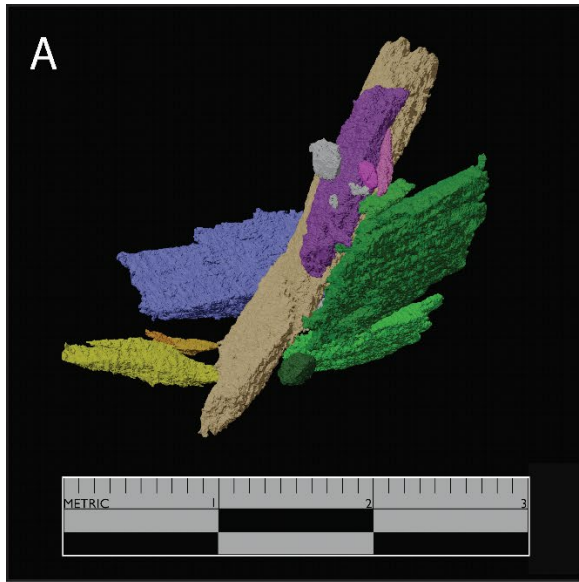
Supplemental Figure 9. Large In Situ Projectile Fragments. A depiction of the pieces embedded in the Manis rib in their original orientation relative to one another; colored pieces were used in the reconstruction while grey pieces were left out. A-D shows the model from four angles as it is rotated clockwise. See Supplemental Table 1 for the sizes of each fragment.

24
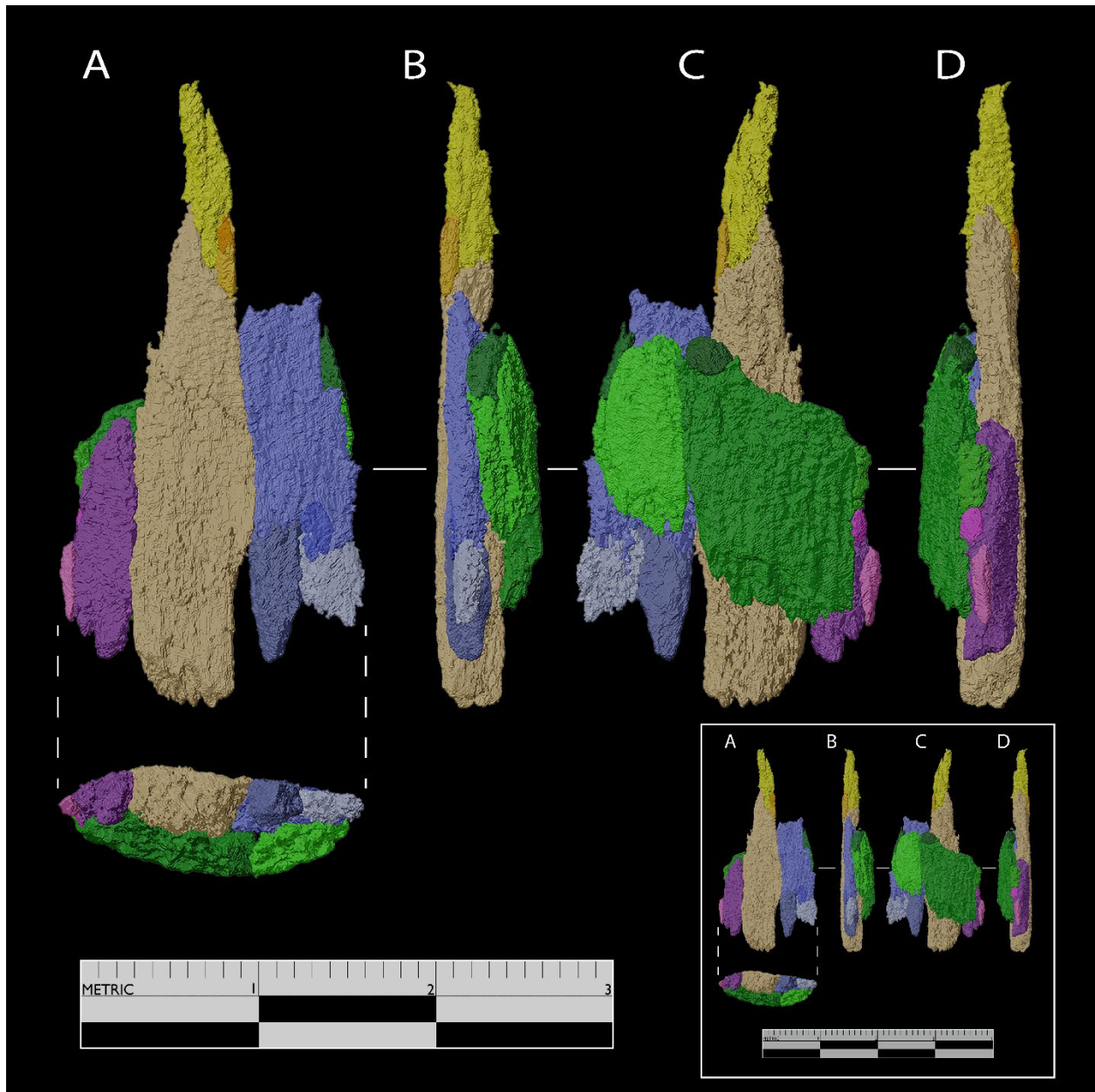
Supplemental Figure 10. Large Scale Manis Osseous Projectile Reconstruction. (A) ventral face, (B) left lateral margin, (C) dorsal face, and (D) right lateral margin. Colors correspond to Supplemental Table 1 and Supplemental Figure 9.